A&A manuscript no.
(will be inserted by hand later)

Your thesaurus codes are:
07(02.14.1; 08.01.1; 08.12.1; 10.05.1; 10.08.1; 10.19.1)

ASTRONOMY AND ASTROPHYSICS

Sc and Mn abundances in disk and metal-rich halo stars ⋆

P.E. Nissen[1], Y.Q. Chen[123], W.J. Schuster[4], and G. Zhao[3]

[1] Institute of Physics and Astronomy, University of Aarhus, DK–8000 Aarhus C, Denmark
[2] Department of Astronomy, Beijing Normal University, Beijing 100875, China
[3] Beijing Astronomical Observatory, Chinese Academy of Sciences, Beijing 100012, China
[4] Observatorio Astronomico National, UNAM, Apartado Postal 877, 22800 Ensenada, B.C., México

Received 7 October 1999 / Accepted 8 November 1999

Abstract. Sc and Mn abundances are determined for 119 F and G main-sequence stars with $-1.4 < [Fe/H] < +0.1$, representing stars from the thin disk, the thick disk and the halo. The results indicate that Sc behaves like an α element, showing a decreasing [Sc/Fe] with increasing metallicity in disk stars and a dual pattern in the kinematically selected halo stars. In contrast, Mn shows an increase from $[Mn/Fe] \simeq -0.5$ at $[Fe/H] = -1.4$ to zero at solar metallicity. There appears to be a discontinuity or sharp increase of [Mn/Fe] at $[Fe/H] \simeq -0.7$ corresponding to the transition between the thick and the thin disk. It is discussed if supernovae of Type Ia are a major source of Mn in the Galactic disk or if the trend of [Mn/Fe] vs. [Fe/H] can be explained by nucleosynthesis in Type II supernovae with a strong metallicity dependence of the yield.

Key words: Nuclear reactions, nucleosynthesis, abundances – Stars: abundances – Stars: late-type – Galaxy: evolution – Galaxy: halo – Galaxy: solar neighbourhood

1. Introduction

Scandium and manganese abundances in long-lived F and G stars are of high interest not only because they help us to understand the chemical evolution of the Galaxy, but also because they provide some special constraints on nucleosynthesis theory.

It has been long known that α elements like O, Mg, Si, and Ca are mostly produced by Type II supernovae, while some iron-peak elements have significant contributions from Type Ia supernovae. But we have no clear idea how Sc, as an element intermediate between α elements and iron-peak elements in the periodic table, is formed. Sc abundances are available only for a few disk stars, and the two most extensive works on halo stars do not give consistent results. Gratton & Sneden (1991) find a solar Sc/Fe ratio in metal-poor dwarfs and giants, while Sc is found to be overabundant by Zhao & Magain (1990) with $[Sc/Fe] \simeq +0.3$ in metal-poor dwarfs. Clearly, more detailed abundance information will be useful to reveal the synthesis history of Sc in the Galaxy.

Mn is known to be quite underabundant with respect to Fe in metal-poor stars (Gratton 1989, McWilliam et al. 1995; Ryan et al. 1996), but the pattern of [Mn/Fe] vs. [Fe/H] is not known in great detail. It is still an open question if Mn is produced mainly in massive stars as advocated by Timmes et al. (1995) or if Type Ia SNe make a significant contribution at higher metallicities. Furthermore, the pattern of [Mn/Fe] in disk and metal-rich halo stars is needed for comparison with recent observations of Mn abundances in damped Lyman α systems (Pettini et al. 1999a; 1999b).

The reason that the Sc and Mn abundance patterns are not well established may be related to the significant hyperfine structure (HFS) of their lines. Data on the HFS of several Sc and Mn lines suitable for abundance determinations of solar-type dwarfs is, however, available. The lack of a consistent study on both elements for disk and metal-rich halo stars therefore inspired us to carry out a high precision analysis for a large sample of main-sequence stars selected to have $5300 < T_{\rm eff} < 6500$ K, $4.0 < \log g < 4.6$, and $-1.4 < [Fe/H] < +0.1$.

2. Observations

The observational data are taken from two sources: Chen et al. (1999, hereafter Chen99) and Nissen & Schuster (1997, hereafter NS97). The first sample (disk stars) was observed at Beijing Astronomical Observatory (Xinglong Station, China) with the Coudé Echelle Spectrograph and a 1024×1024 Tek CCD attached to the 2.16m telescope, giving a resolution of the order of 40 000. The second sample (kinematically selected halo stars and metal-poor disk stars) was observed with the ESO NTT EMMI spectrograph and a 2048×2048 SITe CCD detector at a higher resolution ($R = 60\,000$). The exposure times were chosen in order to obtain a signal-to-noise ratio of above 150 in both samples.

Send offprint requests to: P.E. Nissen

⋆ Based on observations carried out at the European Southern Observatory, La Silla, Chile, and Beijing Astronomical Observatory, Xinglong, China

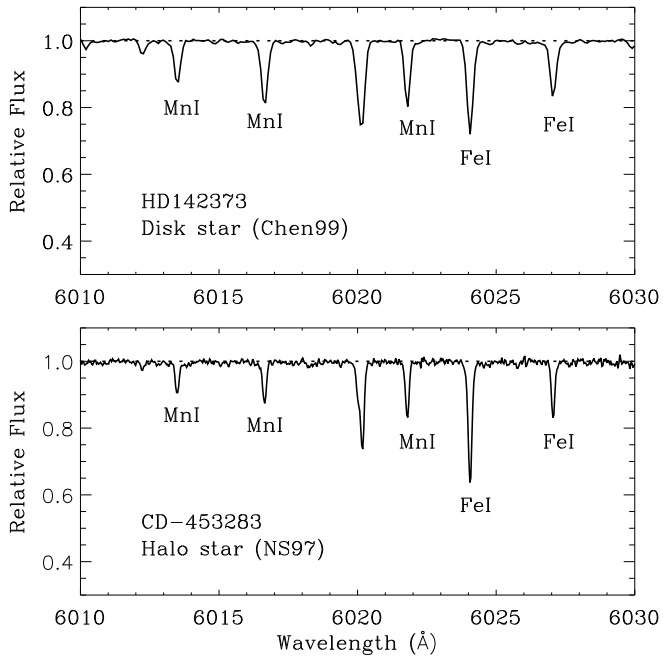

Fig. 1. Examples of spectra for one disk star HD 142373 ($T_{\rm eff}$ = 5920 K, log$g$ = 4.27, [Fe/H] = −0.39) obtained with the 2.16m telescope at Xinglong Station and one halo star CD−45 3283 ($T_{\rm eff}$ = 5650 K, log$g$ = 4.50, [Fe/H] = −0.84) observed at the ESO NTT.

The spectra were reduced with standard MIDAS (Chen99) or IRAF (NS97) routines for background correction, flatfielding, extraction of echelle orders, wavelength calibration, continuum fitting and measurement of equivalent widths (see Chen99 and NS97 for details). Figure 1 shows the spectra for one disk star in Chen99 and one halo star in NS97 around the Mn I triplet at 6020 Å.

3. Analysis

3.1. Abundance calculation

In Chen99, the effective temperature was derived from the Strömgren $b-y$ color index using the recent calibration by the infrared-flux method (Alonso et al. 1996). For consistency, stellar temperatures in the NS97 sample (derived from the excitation balance of Fe I lines) were redetermined using the Alonso et al. calibration of $b-y$. The new $T_{\rm eff}$'s are on the average 60 K lower than those of NS97 but the rms scatter between the two sets of values is only ±45 K.

Surface gravities in Chen99 were based on Hipparcos parallaxes (ESA 1997). For the majority of stars in NS97 accurate parallaxes are, however, not available, and surface gravities were therefore determined by requiring that Fe I and Fe II lines provide the same iron abundance. As shown by Chen99, this leads to gravities consistent with those derived from Hipparcos parallaxes.

Microturbulence velocities were estimated by requesting that the iron abundance derived from Fe I lines with $\chi > 4$ eV should not depend on equivalent width. As shown in Table 2, the typical error of the microturbulence parameter, $\pm 0.3\,{\rm km\,s^{-1}}$, has no significant influence on the derived values of [Sc/Fe] and [Mn/Fe].

The oscillator strengths for two Sc II lines (λ5657 and λ6604) and two Mn I lines (λ6013 and λ6021) were taken from Lawler & Dakin (1989) and Booth et al. (1984), respectively, while differential values for another three Sc II lines and one Mn I line (λ6016) were estimated from an "inverse" analysis of 10 well observed "standard" stars from Chen99 and all stars from NS97. Hence, these lines are forced to give the same average abundances of Sc and Mn as the lines with known gf values for the aforementioned group of stars, but the inclusion of these lines improves the precision of differential abundances. We note, that in the spectrum of the Sun, the Mn I line at 6016 Å appears stronger relative to the two other lines. Hence, this line may be blended by a weak line in metal-rich stars, but exclusion of λ6016 in the derivation of Mn abundances does not change the derived trend of [Mn/Fe] significantly.

The damping constant corresponding to collisional broadening due to Van der Waals interaction with hydrogen and helium atoms was calculated in the Unsöld (1955) approximation with an enhancement factor of $E_\gamma = 2.5$ for both elements. The effect of changing the enhancement factor will be discussed in Sect. 3.3.

The abundance analysis is based on a grid of flux constant, homogeneous, LTE model atmospheres computed using the Uppsala MARCS code with updated continuous opacities (Asplund et al. 1997). Abundance calculations in the LTE approximation with HFS included were made using the Uppsala SPECTRUM synthesis program by forcing the theoretical equivalent widths, derived from the model, to match the observed ones.

Equivalent widths in the solar flux spectrum were measured from a Xinglong spectrum of the Moon and analyzed in the same way as the stellar equivalent widths using the same grid of models to interpolate to the atmospheric parameters of the Sun. Hence, [Sc/Fe] and [Mn/Fe] are derived in a strictly differential way with respect to the Sun, thereby minimizing many error sources. In particular, we emphasize that possible systematic errors in the gf-values do not affect the relative abundance ratios with respect to the Sun.

Table 3 and Table 4 present the derived abundances, together with the atmospheric parameters and equivalent widths, for stars in Chen99 and NS97, respectively.

3.2. Hyperfine structure effect

For all Sc and Mn lines used in our analysis, it was investigated how much the HFS affects the derived abundances. The energy splitting and the relative intensities required in the HFS calculation for Sc and Mn are taken from Stef-

Table 1. The hyperfine structure data for Sc and Mn. χ is the excitation potential of the lower energy level

λ[Å]	χ[eV]	log gf	λ[Å]	χ[eV]	log gf
Sc II			Sc II		
5239.779	1.45	−1.468	5526.777	1.77	−0.858
5239.812	1.45	−1.375	5526.810	1.77	−0.765
5239.845	1.45	−1.583	5526.843	1.77	−0.973
5239.864	1.45	−1.472	5526.862	1.77	−0.862
Sc II			Sc II		
5657.836	1.51	−1.205	6245.576	1.51	−1.736
5657.869	1.51	−1.112	6245.609	1.51	−1.643
5657.902	1.51	−1.320	6245.642	1.51	−1.851
5657.921	1.51	−1.209	6245.661	1.51	−1.740
Sc II			Mn I		
6604.556	1.36	−1.911	6013.537	3.07	−1.365
6604.589	1.36	−1.818	6013.519	3.07	−0.787
6604.622	1.36	−2.026	6013.501	3.07	−1.108
6604.641	1.36	−1.915	6013.486	3.07	−0.977
			6013.474	3.07	−0.767
Mn I			Mn I		
6016.665	3.07	−0.702	6021.814	3.07	−0.477
6016.650	3.07	−1.345	6021.806	3.07	−0.612
6016.638	3.07	−0.683	6021.797	3.07	−0.395
6016.623	3.07	−0.588	6021.780	3.07	−1.225
6016.604	3.07	−1.071	6021.764	3.07	−1.374

fen (1985). His data is mostly based on Biehl (1976), but he makes a small adjustment to the wavelength shift and the relative intensities, leading to fewer components than Biehl's data. The loggf values for the individual components (see Table 1) are then calculated from the relative strengths based on a given total gf value.

The results show that HFS has a small influence on the two weak Sc II lines (λ6245 and λ6604) with a maximum of 0.07 dex at $EW \sim 50$ mÅ, but the effect is very significant for the stronger lines (λ5526 and λ5657), reaching 0.1-0.3 dex for the equivalent width range of 30-100 mÅ. The Sc II 5239Å line (available in the NS97 spectra) is subject to a maximum HFS effect of about 0.1 dex for $EW \sim 50$ mÅ.

For the Mn I lines, the abundance deviation between the derivations with and without HFS reaches a maximum of 0.2 dex for the 6013Å line and 0.10 dex for λ6016 and λ6021 at $EW \sim 100$ mÅ. We have found that the HFS data of Booth et al. (1983) gives slightly lower Mn abundances than Steffen's (1985) data; the deviation increases with line strength, reaching 0.1 dex for the 6013Å line and 0.04 dex for λ6016 and λ6021 at $EW \sim 100$ mÅ. The reason for the discrepancy is unclear. But the original HFS data for λ6013 from Biehl (1976) gives exactly the same abundance as that based on Steffen's (1985) HFS data.

The final abundances are the mean values of the abundances derived from the available lines with HFS according to Steffen (1985) taken into account.

3.3. Abundance uncertainties

Abundance errors are mainly due to random errors in the equivalent widths, the uncertainty of the stellar atmospheric parameters, and a possible error in the enhancement factor of the damping constant. An estimate of the first contribution is obtained by dividing the rms scatter of abundances, determined from the individual lines, by $\sqrt{N}$, where N is the number of lines. The second kind of uncertainty is estimated by a change of 70 K in $T_{\rm eff}$, 0.1 dex in log$g$, 0.1 dex in [Fe/H] and 0.3 km s^{-1} in microturbulence, typical standard deviations for these atmospheric parameters as estimated in Chen99. Finally, the abundance change caused by a variation of E_γ by 50% was calculated.

Table 2 presents the errors in the relative abundances for a typical disk star and one of the halo stars. Note, that we have compared the Sc abundance derived from Sc II lines with the Fe abundance derived from Fe II lines and the Mn abundance derived from Mn I lines with the Fe abundance derived from Fe I lines. Hence, the ratios are derived from lines having a similar dependence on $T_{\rm eff}$ and log$g$, which explains the the rather small effect of the uncertainty in the atmospheric parameters. In the case of Sc the uncertainty of the enhancement factor is not important, because the Sc II lines are quite weak and not of too different strenghts in the solar and the stellar spectra. The Mn I lines show, however, a large variation in equivalent width, from about 100 mÅ at solar metallicity to about 10 mÅ in the metal-poor halo stars (due to the underabundance of Mn with respect to Fe). Hence, the choice of E_γ has a significant effect on the slope of [Mn/Fe] vs. [Fe/H]. As seen from Table 2, an increase of E_γ by 50% (from 2.5 to 3.75) increases the derived [Mn/Fe] at [Fe/H] ~ -0.8 by 0.05 dex, and a decrease of E_γ from 2.5 to 1.0 (i.e. no enhancement of the Unsöld approximation for the damping constant) would decrease [Mn/Fe] of the metal-poor stars by about 0.10 dex. Unfortunately, there are no reliable theoretical calculations of the damping constant for the Mn I lines, nor any empirical estimates of E_γ from e.g. the solar spectrum.

In addition to the abundance errors estimated in Table 2, possible non-LTE effects should be considered. As the Sc abundance is determined from Sc II lines and compared to Fe from Fe II lines, the non-LTE effects on [Sc/Fe] should be small, because the abundances of both elements are based on lines from the dominating ionization stage. The Mn abundances (derived from Mn I lines) may, however, be subject to non-LTE effects due to overionization of Mn I caused by the UV radiation field, especially in the metal-poor stars. According to our knowledge there is no non-LTE calculations of Mn for F and G stars, but noting that the ionization potential of Mn I (7.43 eV) is similar to that of Fe I (7.87 eV) one might expect that the ratio Mn/Fe is not significantly changed by non-LTE effects, when the abundances of both elements are deter-

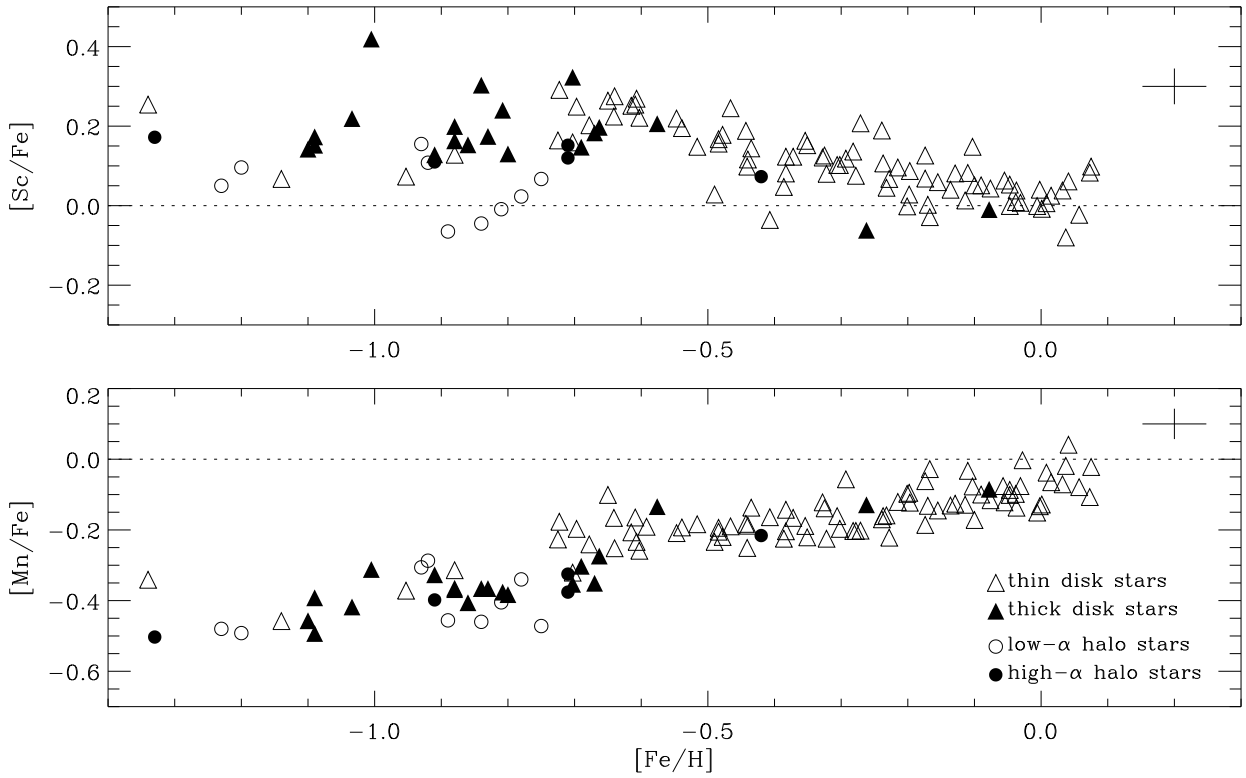

Fig. 2. Abundance patterns for Sc and Mn in four groups of stars.

Table 2. Abundance errors for HD 142373 and CD−45 3283. The atmospheric parameters of the stars are given in connection with Fig. 1

	HD 142373		CD−45 3283	
	$\Delta[\frac{\rm Sc}{\rm Fe}]$	$\Delta[\frac{\rm Mn}{\rm Fe}]$	$\Delta[\frac{\rm Sc}{\rm Fe}]$	$\Delta[\frac{\rm Mn}{\rm Fe}]$
$\frac{\sigma_{EW}}{\sqrt{N}}$	0.033	0.037	0.045	0.042
$\Delta T_{\rm eff} = +70$K	0.023	0.002	0.011	0.017
$\Delta \log g = +0.1$	−0.001	−0.002	−0.006	0.003
Δ[Fe/H] $= +0.1$	0.004	0.001	0.004	0.003
$\Delta\xi = +0.3$	−0.011	0.008	0.008	0.018
$\Delta E_\gamma = +50\%$	0.002	0.040	0.006	0.052

mined from neutral lines. Clearly, this should be checked by detailed computations.

4. Discussion and conclusions

Stars in the metallicity range $-1.4 <$ [Fe/H] $< +0.1$ include a mixture of different populations. In our sample, three groups can be separated according to their kinematics: thin disk stars ($V' > -50\,{\rm km\,s^{-1}}$), thick disk stars ($-120 < V' < -50\,{\rm km\,s^{-1}}$) and halo stars ($V' < -175\,{\rm km\,s^{-1}}$). The values of V'(the velocity component in the direction of Galactic rotation with respect to the Local Standard of Rest) are taken from Chen99 and NS97. As discussed in Chen99 a rotational lag of about $50\,{\rm km\,s^{-1}}$ corresponds rather well to the transition between thick disk stars ($\sigma(W') \sim 40\,{\rm km\,s^{-1}}$ and ages > 10 Gyr) and thin disk stars ($\sigma(W') \sim 20\,{\rm km\,s^{-1}}$ and ages < 10 Gyr) although a clean separation between the two populations is not possible. The thick disk stars may also be contaminated by a few halo stars, whereas the group with $V' < -175\,{\rm km\,s^{-1}}$ consists of genuine halo stars according to the Galactic orbits computed in NS97. Furthermore, the halo stars can be split up into "low-α" and "high-α" stars according to the abundances of α elements as described by NS97. The low-[α/Fe] halo stars may belong to the "high-halo", resulting from a merging process of the Galaxy with satellite components (NS97), or they may come from low-density regions in the outer halo where the chemical evolution proceeded slowly allowing incorporation of iron from Type Ia SNe at a lower metallicity than in the inner halo and the thick disk (NS97; Gilmore & Wyse 1998).

Figure 2 shows the run of [Sc/Fe] and [Mn/Fe] vs. [Fe/H] with the four groups of stars marked by different symbols.

4.1. Scandium

As seen from Fig. 2, [Sc/Fe] declines from an overabundance (~ 0.2) at [Fe/H] $= -1.4$ to zero at solar metallicity even though there are some exceptions. Hence, Sc seems to follow the even-Z α elements like Si, Ca and Ti (see Ed-

vardsson et al. 1993 and Chen99). In particular, Sc keeps a near-constant overabundance for [Fe/H] < -0.6 like the α elements, except for the group of low-[α/Fe] halo stars, which tend to have low values of [Sc/Fe], just as expected if Sc belongs to the α-element family.

Theoretically, Samland's (1998) model reproduces both the overabundance of about 0.2 dex in [Sc/Fe] at [Fe/H] ~ -1.0 and the decreasing relation with increasing metallicity by suggesting that Sc is mostly made by high mass stars. Observationally, our result supports the high values of [Sc/Fe] for metal-poor dwarfs by Zhao & Magain (1990) instead of the solar ratio found by Gratton & Sneden (1991) for metal-poor dwarfs and giants. The reason for this discrepancy is unclear, but we note that Gratton & Sneden adopt solar gf values based on the empirically-derived solar model by Holweger & Müller (1974). As stated in their paper, the use of a theoretical model for the Sun (like for the stars) would increase the derived [Sc/Fe] values by 0.06 dex. Furthermore, we note that Hartmann & Gehren (1988) derive an average value [Sc/Fe] $= +0.11$ for 16 metal-poor subdwarfs.

4.2. Manganese

Figure 2 shows that [Mn/Fe] increases from a very significant underabundance at [Fe/H] ~ -1.4 to a solar ratio at [Fe/H] $\simeq 0.0$. The underabundance of ~ -0.5 in the metal-poor stars is consistent with the recent study of Mn in damped Lyman-α systems by Pettini et al. (1999a; 1999b), and with the results of Gratton (1989), who found [Mn/Fe] ~ -0.4 in 11 giants and dwarfs with $-2.5 <$ [Fe/H] < -1.0 and an increasing trend of [Mn/Fe] with [Fe/H] for 14 disk stars.

Timmes et al. (1995) have shown that nucleosynthesis of Mn in massive stars with a metallicity dependent yield (due to the lower neutron excess in metal-poor stars) explains the trend of [Mn/Fe] rather well, and they argue that Type Ia SNe are not a major contributor to the synthesis of Mn. As seen from Fig. 2 there is, however, a rather sharp increase of [Mn/Fe] around [Fe/H] ~ -0.7 or even a discontinuity in [Mn/Fe] between the thick disk and halo stars on one side and the thin disk stars on the other side. In fact, the trend of [Mn/Fe] appears to mirror that of the α elements, especially that of O (Edvardsson et al. 1993; Chen99). This suggests that Type Ia SNe give a large contribution to the production of Mn in the Galactic disk in agreement with the chemical evolution model of Samland (1998), who finds that 75% of the Galactic Mn is produced in SNe of Type Ia. On the other hand, we note that the "low-α" halo stars do not stand out from the thick disk stars in the [Mn/Fe] – [Fe/H] diagram. If Type Ia SNe make a large contribution to the production of Mn one might expect the "low-α" stars to have higher [Mn/Fe] values than the thick disk stars, because the "low-α" stars were explained by assuming that they were formed from interstellar gas enriched at lower than usual [Fe/H] values with the products of Type Ia supernovae. However, the position of the "low-α" stars in Fig. 2 may be due to cancelling effects; the Type Ia SNe produce no O and fewer α-elements than Type II SNe, and the neutron excess necessary for Mn production may depend more on the overall metallicity than on just [Fe/H].

We conclude that the nucleosynthesis of Mn may be modulated in a complicated way. Moreover, it is hard to understand why a strong underabundance like that of Mn is not present for the other odd-Z iron-peak elements, V and Co. According to the results of Gratton & Sneden (1991), it seems that V and Co vary in lockstep with Fe down to metallicities of [Fe/H] $\simeq -2.5$, perhaps with a slight underabundance of Co. Furthermore, Mn and Co show very different behaviours below [Fe/H] $\simeq -2.5$ (McWilliam et al. 1995; Ryan et al. 1996) with [Mn/Fe] decreasing strongly and [Co/Fe] increasing. Hence, the term "iron-peak" elements does not indicate the products of a single nuclear reaction. These elements may have different origins. Further study of Mn and of other "iron-peak" elements is desirable to understand their synthesis.

Acknowledgements

This research was supported by the Danish Research Academy and the Chinese Academy of Science, and by CONACyT and DGAPA, UNAM in México.

References

Alonso A., Arribas S., Martínez-Roger C. 1996, A&A 313, 873
Asplund M., Gustafsson B., Kiselman D., Eriksson K. 1997, A&A 318, 521
Biehl D., 1976, Diplomarbeit, Inst. f. Theor. Physik. u. Sternwarte, Kiel University
Booth A.J., Blackwell D.E., Petford A.D.,Shallis M.J. 1984, MNRAS, 208, 147
Booth A.J., Shallis M.J., Wells M., 1983, MNRAS, 205, 191
Chen Y.Q., Nissen P.E., Zhao G., Zhang H.W., Benoni T., 1999, A&AS, in press (Chen99)
ESA 1997, The Hipparcos and Tycho Catalogues, ESA SP-1200
Edvardsson B., Andersen J., Gustafsson B., Lambert D.L., Nissen P.E., Tomkin J. 1993, A&A 275, 101
Gilmore G., Wyse R.F.G. 1998, AJ 116, 748
Gratton R.G. 1989, A&A 208, 171
Gratton R.G., Sneden C., 1991, A&A 241, 501
Hartmann K., Gehren T. 1988, A&A 199, 269
Holweger H., Müller E.A. 1974, Solar Phys. 39, 19
Lawler J.E., Dakin J.T. 1989, J. Opt. Soc. Am. B6, 1457
McWilliam A., Preston G.W., Sneden C., Searle L. 1995, AJ 109, 2757
Nissen P.E., Schuster W.J. 1997, A&A 326, 751 (NS97)
Pettini M., Ellison S.L., Steidel C.C., Bowen D.V. 1999a, ApJ 510, 576
Pettini M., Ellison S.L., Steidel C.C., Shapley A.E., Bowen D.V. 1999b, ApJ, in press
Ryan S.G., Norris J.E., Beers T.C. 1996, ApJ 471, 254
Samland M. 1998, ApJ 496, 155
Steffen M. 1985, A&AS, 59, 403

Timmes F.X., Woosley S.E., Weaver T.A. 1995, ApJS 98, 617
Unsöld A. 1955, Physik der Sternatmosphären, Springer-Verlag, Berlin.
Zhao G., Magain P. 1990, A&A 238, 242

Table 3. Atmospheric parameters, relative abundance ratios, and equivalent widths in mÅ for 4 Sc II and 3 Mn I lines for stars from Chen99.

Star (HD)	$T_{\rm eff}$	log$g$	[$\frac{\rm Fe}{\rm H}$]	[$\frac{\rm Sc}{\rm Fe}$]	[$\frac{\rm Mn}{\rm Fe}$]	λ5526	λ5657	λ6245	λ6604	λ6013	λ6016	λ6021
SUN	5780	4.44	0.00	0.00	0.00	80.6	71.6	38.4	39.3	92.7	100.5	99.0
400	6122	4.13	−0.23	0.05	−0.16		71.0	30.8	34.8	45.7	65.4	53.9
3454	6056	4.29	−0.59		−0.19		55.5	22.2			32.8	40.6
5750	6223	4.21	−0.44	0.12	−0.19		54.2	25.0			40.7	40.3
6834	6295	4.12	−0.73	0.29	−0.18		48.3	22.6		13.3	25.5	
6840	5860	4.03	−0.45	0.19	−0.18		71.4	39.8	31.4	45.4	53.2	60.4
10307	5776	4.13	−0.05		−0.08		77.1	43.3	41.5	84.1	98.5	92.4
11007	6027	4.20	−0.16	0.06	−0.14		61.8	42.2	34.1	56.6	65.9	
11592	6232	4.18	−0.41	−0.04	−0.16		60.0	13.9		34.3	37.9	
19373A	5867	4.01	0.03	0.04	−0.07		85.9	49.7	51.7	86.5		95.9
22484	5915	4.03	−0.13	0.08	−0.13		81.0	42.7	44.1	67.4	80.5	80.6
24421	5986	4.10	−0.37	0.12	−0.17		71.4	28.5	31.2	43.5	52.5	57.9
25173	5867	4.07	−0.62	0.25	−0.17		64.4	30.2	28.1	28.8	44.4	49.9
25457	6162	4.28	−0.11	0.05	−0.17			29.9	39.5	62.3	70.8	71.4
25998	6147	4.35	−0.11	0.15	−0.08			36.1	44.9		89.4	87.9
33632A	5962	4.30	−0.23	0.07	−0.22		64.4	30.4	29.3	43.5	64.7	64.7
34411A	5773	4.02	0.01	0.01	−0.04		83.8	45.3	46.2	89.3		99.0
35296A	6015	4.24	−0.14	0.04	−0.13	81.0			34.0		81.5	72.6
39587	5805	4.29	−0.18	0.13	−0.06	74.9	76.1	32.1	33.2	87.4	87.6	87.4
39833	5767	4.06	0.04	−0.08	−0.02	82.8	77.3	43.2	43.0	95.1		
41640	6004	4.37	−0.62	0.25	−0.21		56.3	23.2	20.9	30.7	31.8	38.1
43947	5859	4.23	−0.33	0.13	−0.14	73.6		30.7	26.8	60.3	62.1	65.5
46317	6216	4.29	−0.24	0.19	−0.17	93.0	75.9	32.3	30.0	43.7	51.8	53.5
49732	6260	4.15	−0.70	0.25	−0.20			21.0	18.5	19.3		25.2
54717	6350	4.26	−0.44	0.14	−0.14	61.2	57.6	23.5	22.6	35.0	34.5	35.4
55575	5802	4.36	−0.36	0.16	−0.19	72.5	61.2	33.1	30.0	52.7	60.3	64.8
58551	6149	4.22	−0.54	0.19	−0.19	70.6	56.8	23.5	20.3	30.1	33.2	37.8
58855	6286	4.31	−0.31	0.10	−0.16		63.3	26.5	24.3	38.7	44.6	48.8
59380	6280	4.27	−0.17	0.00	−0.13	74.1		27.6	26.8	48.1	59.4	59.8
59984A	5900	4.18	−0.71	0.16	−0.32	61.3	54.7	25.0	24.6		29.6	29.8
60319	5867	4.24	−0.85	0.30	−0.37	54.8	49.7	21.0	17.3	13.7	19.0	26.8
62301	5837	4.23	−0.67	0.20	−0.27	63.2	55.5	27.2	23.2	25.7	33.9	38.7
63333	6057	4.23	−0.39	0.12	−0.14	68.0	63.7	26.1	29.1	48.5	47.7	50.4
68146A	6227	4.16	−0.09	0.05	−0.10	85.8	84.6	38.6	33.0	63.0	65.5	70.4
69897	6243	4.28	−0.28	0.14	−0.20	73.3	80.0	29.1	25.4	40.6	44.7	48.7
72945A	6202	4.18	0.00	0.00	−0.15	91.6	84.0	39.4	35.2		77.2	76.7
75332	6130	4.32	0.00	−0.01	−0.13	86.5	82.0	31.6	36.8	76.8	81.8	77.7
76349	6004	4.21	−0.49	0.17	−0.19	77.5	61.8	26.7	21.2	34.0	43.8	49.3
78418A	5625	3.98	−0.26	−0.06	−0.13	64.6	68.3	33.6	34.5	73.6	76.7	74.0
79028	5874	4.06	−0.05	0.05	−0.09	92.1	90.8	46.3	48.3	84.3	90.8	87.0
80218	6092	4.14	−0.28	0.08	−0.20	78.3	64.6	37.0	27.5		55.0	53.7
89125A	6038	4.25	−0.36	0.15	−0.22	72.7	73.5	29.8	25.3		46.7	52.8
90839A	6051	4.36	−0.18	0.07	−0.19	77.1	67.5	33.7	30.4	56.4	67.4	65.2
91889A	6020	4.15	−0.24	0.11	−0.16	87.1	71.9	33.8	34.6	51.6	59.6	62.7
94280	6063	4.10	0.06	−0.02	−0.08	94.3	86.8	47.3	37.5	82.0	92.7	83.9
95128	5731	4.16	−0.12	0.08	−0.03		77.4	42.2	40.8	94.7	95.8	90.9
97916	6445	4.16	−0.94	0.07	−0.37			8.1				10.4
100180A	5866	4.12	−0.11	0.01	−0.13	88.9	76.4	36.0	34.4	72.2	84.7	82.7
100446	5967	4.29	−0.48	0.18	−0.22	66.1	60.9	26.4	25.5	32.4	44.7	0.0
100563	6423	4.31	−0.02		0.00					70.9		75.8
101676	6102	4.09	−0.47	0.25	−0.19	94.4	64.1	28.7	32.2	33.5	42.1	40.6
106516A	6135	4.34	−0.71	0.32	−0.35	62.1	48.9	22.3	19.9	16.0	20.3	18.8
108510	5929	4.31	−0.06	0.06	−0.12	90.2	78.1	38.5	34.7	78.7	86.5	84.2
109303	5905	4.10	−0.61	0.27	−0.23	73.6	68.7	24.7	30.9		34.2	44.6
114710A	5877	4.24	−0.05	0.00	−0.10	81.7	73.6	37.2	34.8	81.0	87.1	86.9

Table 3.(continued)

Star (HD)	$T_{\rm eff}$	log$g$	$[\frac{\rm Fe}{\rm H}]$	$[\frac{\rm Sc}{\rm Fe}]$	$[\frac{\rm Mn}{\rm Fe}]$	λ5526	λ5657	λ6245	λ6604	λ6013	λ6016	λ6021
115383A	5866	4.03	0.00	0.04	−0.13	97.4	99.8	45.9	43.8			96.3
118244	6234	4.13	−0.55	0.22	−0.21	78.4	58.2	22.5	24.8	27.2	30.3	31.9
121560	6059	4.35	−0.38	0.08	−0.20	73.8	53.5	24.5	22.1	35.8	49.5	49.2
124244	5853	4.11	0.05	0.06	0.04		85.2	50.0	48.9	96.9		
128385	6041	4.12	−0.33	0.12	−0.12	75.4	74.2	34.9	31.6	48.5	54.4	64.9
130948	5780	4.18	−0.20	0.03	−0.09	82.9	70.4	34.8	30.1	80.0	84.5	85.4
132254	6231	4.22	0.07	0.08	−0.11	97.3	96.4	43.7	47.3	72.4	80.0	79.8
139457	5941	4.06	−0.52	0.15	−0.18		64.8	23.3	29.7		43.0	52.2
142373	5920	4.27	−0.39	0.05	−0.22	71.6	66.9	31.9		36.5	55.5	52.8
142860A	6227	4.18	−0.22	0.10	−0.12				31.4	51.4	56.3	59.5
146099A	5941	4.10	−0.61	0.22	−0.26		63.1	25.4		29.0	32.9	36.9
149750	5792	4.17	0.08	0.10	−0.02			51.1		99.2		
154417	5925	4.30	−0.04	0.01	−0.10	83.1	75.2	34.3	34.2	76.3	90.2	85.6
157347	5654	4.36	−0.02	0.01	−0.08		72.3	38.3		94.6		
157466	5935	4.32	−0.44	0.10	−0.25		54.7	23.9		37.3	46.5	50.1
162004B	6059	4.12	−0.08	0.04	−0.12		84.7	41.9	36.8	69.5		82.2
167588	5894	4.13	−0.33	0.08	−0.22		72.5	39.5	37.1	44.4	57.6	60.7
168009	5719	4.08	−0.07	−0.01	−0.09		78.5	40.1	37.2	84.6		97.1
170153A	6034	4.28	−0.65	0.26	−0.10		44.6	23.8	29.7		43.6	40.8
184601	5830	4.20	−0.81	0.24	−0.38		48.5	19.3	18.7	13.5	25.1	27.0
189340	5888	4.26	−0.19	0.09	−0.12		67.0	33.6	40.7	68.4	80.8	83.6
191862A	6328	4.19	−0.27	0.21	−0.20		74.4	38.3	39.9	37.9	45.2	51.7
198390	6339	4.20	−0.31	0.10	−0.20		67.2		24.4	39.4	43.8	34.1
200580	5829	4.39	−0.58	0.21	−0.13		51.7	21.0	25.9	32.6	56.6	53.3
201891	5827	4.43	−1.04	0.22	−0.42		29.7	18.0	8.7	9.7		15.9
204306	5896	4.09	−0.65	0.28	−0.25		58.1	31.8	27.5	24.0	34.6	40.1
204363	6141	4.18	−0.49	0.16	−0.20		54.5	25.6	26.5	29.4	36.0	42.2
206301	5682	3.98	−0.04	0.04	−0.14		85.6	54.6	46.8	94.0		96.5
206860	5798	4.25	−0.20	0.00	−0.10		65.5		30.6	73.6	92.9	87.7
208906A	5929	4.39	−0.73	0.16	−0.23		38.8	15.8	17.7	20.6	31.9	34.5
209942A	6022	4.25	−0.29	0.12	−0.06		67.6	36.4	28.4	54.2	78.9	67.1
210027A	6496	4.25	−0.17	−0.03	−0.03		60.1	24.4		48.4	62.0	46.0
210752	5847	4.33	−0.68	0.20	−0.24		45.3	16.8	27.3	30.1	33.9	41.6
212029A	5875	4.36	−1.01	0.42	−0.31		35.9	20.1	17.6	18.9	11.6	18.1
215257	5976	4.36	−0.65	0.22	−0.17		50.6			23.6	49.3	34.0
219623A	6039	4.07	0.02	0.03	−0.06		80.4	40.5	39.8	77.4	98.1	73.7

Table 4. Atmospheric parameters, relative abundance ratios, and equivalent widths in mÅ for 5 Sc II and 3 Mn I lines for stars from NS97

Star	$T_{\rm eff}$	log$g$	$[\frac{\rm Fe}{\rm H}]$	$[\frac{\rm Sc}{\rm Fe}]$	$[\frac{\rm Mn}{\rm Fe}]$	λ5239	λ5526	λ5657	λ6245	λ6604	λ6013	λ6016	λ6021
BD−21 3420	5858	4.25	−1.09	0.17	−0.49	18.4	37.7	28.0	10.2	11.5	8.1	9.4	10.5
CD−33 3337	6022	3.99	−1.34	0.25	−0.34	17.1	37.1	26.1	7.9	8.0	4.6	6.8	8.0
CD−45 3283	5650	4.50	−0.84	−0.05	−0.46	18.0	33.3	23.1	8.0	10.1	16.0	21.6	28.3
CD−47 1087	5657	4.20	−0.80	0.13	−0.38	32.5	53.8	43.5	18.6		20.2	27.0	32.8
CD−57 1633	5944	4.22	−0.89	−0.06	−0.45	17.7	36.1	24.3	7.9	8.9	9.5	13.9	18.4
CD−61 0282	5772	4.20	−1.23	0.05	−0.48	11.8	25.6	19.3	6.6	7.8	6.0	7.4	11.4
G005−040	5737	4.02	−0.91	0.11	−0.39	31.4	54.7	35.8	18.8	17.4	14.2	18.2	26.0
G046−031	5907	4.18	−0.81	−0.01	−0.40	23.6	45.5	33.3	11.9	11.3	13.4	19.0	23.2
G088−040	5911	4.14	−0.83	0.17	−0.36	30.4	59.3	43.9	17.9	19.1	14.1	19.1	24.6
G102−020	5310	4.56	−1.09	0.15	−0.39	18.9	34.0	26.7	9.5	10.9	17.3	19.0	32.1
HD 3567	6041	4.01	−1.20	0.10	−0.49	15.2	34.4	22.7	6.6	9.1	4.0	5.7	9.0
HD 17288	5700	4.38	−0.88	0.20	−0.36	28.3	49.7	38.6	14.4	16.0	17.6	21.7	28.7
HD 17820	5750	4.11	−0.69	0.15	−0.30	40.8	66.9	56.4	22.7	22.6	25.0	32.8	38.8
HD 22879	5774	4.20	−0.86	0.15	−0.40	30.4	53.5	39.5	16.4	16.8	15.4	19.7	23.8
HD 24339	5810	4.20	−0.67	0.18	−0.35	41.2	68.0	54.0	23.0	23.2	22.1	29.3	35.1
HD 25704	5765	4.12	−0.91	0.13	−0.32	27.8	51.0	39.4	16.2	15.4	16.3	20.2	27.2
HD 76932	5849	4.11	−0.88	0.16	−0.36	30.4	55.6	42.8	17.5	17.2	13.5	18.7	24.3
HD 83220	6470	4.06	−0.49	0.03	−0.23		66.3	52.9	18.3	18.5		25.4	28.3
HD103723	6062	4.33	−0.75	0.07	−0.47	23.6	48.7	36.6	13.6	12.4	11.3	14.8	18.4
HD105004	5832	4.32	−0.78	0.02	−0.34	25.4	44.9	33.0	11.7		17.1	25.9	29.0
HD106038	5939	4.23	−1.33	0.17	−0.50	13.1	29.5	18.3	6.1	4.8		4.2	8.0
HD113083A	5867	4.35	−0.93	0.16	−0.30	22.0	42.2		12.1	10.8	14.7	18.1	24.8
HD113083B	5768	4.34	−0.91	0.11	−0.28	22.4	43.7	29.3	11.9	12.1	17.9	22.7	29.6
HD113679	5595	3.98	−0.71	0.15	−0.32	47.8	71.0	57.8	29.0	29.9	27.5	36.7	41.6
HD120559	5405	4.40	−0.88	0.13	−0.31	25.1	45.8	35.6	13.5	16.1	26.2	34.3	43.9
HD121004	5622	4.31	−0.71	0.12	−0.37	33.7	56.2	46.2	19.8		24.1	31.9	39.0
HD126681	5533	4.28	−1.14	0.07	−0.45	15.9	31.2	24.8	7.3	9.8	9.8	15.4	18.8
HD241253	5830	4.23	−1.10	0.14	−0.45	19.1	37.0	28.0	8.5	10.8	8.1	9.0	14.2
W7547	6272	4.03	−0.42	0.07	−0.21	49.8	78.1	66.0	32.5	27.2	27.7	35.3	40.2